4-23-2007

On the Removal of Iron-Peak Nuclei from the Surface of the Crab Pulsar

Steven J. Vanderveer
Trinity University

On the Removal of Iron-Peak Nuclei from the Surface of the Crab Pulsar

Steven J. Vanderveer

Thesis Presented to the Faculty of Trinity University, San Antonio
for Completion of the Bachelor of Science Degree with Honors

April 23, 2007

Abstract

The Crab Nebula contains a number of regions of anomalous elemental abundances, including a large band of nearly pure helium and several pockets that display unusually strong nickel lines. Previous attempts at their explanation have proven unsatisfactory, so we turn our focus to the pulsar which powers the nebula. Following the suggestion that positive ions could be removed from the surface of the central neutron star (rich in iron-peak nuclei), we have examined this possibility within the framework of the Ruderman & Sutherland polar gap magnetospheric model. We identify two processes, surface irradiation by electrons and subsurface electron flows, that, owing to the Crab Pulsar's youth, appear to raise the surface temperature of the magnetic polar cap region to levels at which significant thermionic emission of iron-peak nuclei occurs.

Figure 1: False color X-ray image of the Crab Nebula. The arrow indicates the position of the pulsar. We note two jets leading away from the pulsar toward the upper right and the lower left of the image. These reveal the pulsar's magnetic poles and give us a sense of orientation of the neutron star relative to the nebula. The prominent high-energy torus (in blue) appears to be in the pulsar's equatorial plane. This is distinct from the helium torus discussed in this paper, which is not visible in this image. Image: NASA, Chandra X-Ray Observatory

Contents

Introduction

Young supernova remnants, such as the Crab Nebula, provide a rare opportunity to study nucleosynthesis and other elemental processing that takes place within the core of an active star. A great deal of additional elemental processing takes place during and after the supernova event, producing metals beyond the iron-peak. The Crab Nebula, in particular, provides a wealth of information about these important processes. It has been linked to the (Type II) supernova event recorded by Chinese and Arab astronomers in the year 1054 C.E. It is centered about a highly energetic pulsar which provides sufficient power that the nebula emits primarily via synchrotron radiation (MacAlpine et al. 1996). In addition to its youthful high energy, the Crab Nebula is also important in the investigation of the origin of elements because it is relatively nearby. Additionally, it sits about 180 parsecs away from the galactic plane, significantly increasing the likelihood that the observed material originated in the progenitor star (or subsequent intra-nebular processing) and is unadulterated by interstellar media (MacAlpine et al. 2007).

There have been several surveys of the structure and composition of the Crab Nebula (Miller 1978; Fesen & Kirshner 1982; Henry 1984; Uomoto & MacAlpine 1987; MacAlpine 1989; MacAlpine & Uomoto 1991; MacAlpine et al. 1996; MacAlpine et al. 2007). Together, they indicate that the nebula alone contains less than 2 solar masses of visible material, most of which is helium. This is unusual among supernova remnants. There is also a strong nitrogen presence, suggesting the helium was produced through the CNO-cycle. Roughly 25% of the helium is contained in a torus that stretches east-west, appearing to cover the pulsar. There is also a nitrogen-poor/sulfur-rich area just south of the pulsar, indicating that shell oxygen-burning took place in the progenitor star pre-supernova. Remaining anomalies include pockets extremely rich in [C I] (upwards of 7 times more than expected based on models), as well as areas producing strong [Ni II] $\lambda 7378$ lines, believed to be neutron-rich nickel some 5-50 times more abundant than solar values. The nickel also seems to be paired with iron emissions, though the latter are much less enhanced; the nickel/iron ratio is roughly 60-75 times solar (MacAlpine et al. 2007), such that iron abundances are less than solar levels. This is likely due to the association of iron and dust in the nebula. We choose to investigate the departure of iron from the neutron star surface in this paper because of the availability of binding energy calculations for iron in the literature, and because the conclusions made for iron are easily generalized to similiar iron-peak and nickel nuclei.

As for the helium observed in the nebula, the bulk of it likely originated as ejecta from the inner mantle of the progenitor star in the course of the supernova event. The formation of the helium torus and the origin of the nickel, however, are only weakly understood. MacAlpine et al. (2007) suggest that the surface of the neutron star is a source of the heavy nuclei (like nickel). Ruderman & Sutherland (1975), representing the standard model for pulsar magnetospheres, argue that positive ions cannot be lifted from the surface of a neutron star, except possibly in the case of young, hot remnants, like that found in the Crab Nebula. We seek to evaluate the plausibility of this scenario. Section 1 is a brief sketch of the changes that occur when a star undergoes Type II supernova, as well as an outline of the properties of the Crab pulsar that will be used in all calculations that follow. In Section 2 we examine arguments given by Michel (1975) that the iron lattice which makes up the surface of a neutron star must also be covered with a thin layer of helium. If this is the case, its subsequent ejection could be an explanation for the odd helium torus. It is important to note that Michel does not work under Ruderman & Sutherland's so-called "standard model," which is presented in Section 3 along with comments concerning its applicability. We then turn

our attention to the anomalous nickel, which we approach by first examining determinations of the binding energy of iron at the neutron star surface that are in the literature. This is done in Section 4. Section 5 examines the ability of cascades of electrons produced in the magnetosphere and flows of electrons under the surface to provide sufficient heat that positive ions may be thermionically emitted. Utilizing these heat sources, we calculate the amount of iron emitted from the surface over the Crab's lifetime in Section 6, allowing us to speculate on surface nickel and its emission into the nebula.

1 Supernovae and the Crab Nebula

Supernovae are so named because they appear in the night (and sometimes day) sky as brilliant, sustained flashes where there had previously been little or no light observed; they seem as if a new star has been born. The reality is actually quite the opposite, as supernovae herald the explosive deaths of either white dwarfs or massive main-sequence stars. The former are known as Type I Supernovae, occurring when a binary white dwarf, whose companion star has remained on the main sequence, pulls enough material onto its surface from its companion to reignite fusion in its degenerate core. The massive outflux of energy tears the dwarf apart in a supernova. Isolated stars may undergo Type II supernovae, but they must leave the main sequence with the right mass: a minimum of 8 - 11 $M_\odot$.

1.1 The Death of Massive Stars

All stars begin life as a massive cloud of (mostly) hydrogen which has self-attracted to form a spherical object. The cloud collapses until the temperature in its core has escalated to the point that sustainable fusion spontaneously occurs. This thermonuclear fusion process provides the necessary energy to balance the tremendous force of self-gravity attempting to further collapse the newly birthed star. Stars near the lower end of the mass scale, such as our Sun, spend most of their energy-generating lives converting hydrogen into helium in their cores. When the core hydrogen has been completely consumed, helium-burning begins in the core. Lower mass stars cannot achieve the core temperatures necessary to begin burning the products of helium fusion (carbon and oxygen), so gravity is suddenly unbalanced. Further collapse ensues until an object-wide degenerate electron state forms, the pressure of which can offset the object's own gravity.

Stars that are massive enough to burn carbon and oxygen within their cores do so. Meanwhile, the mantle hydrogen closest to the core is sufficiently heated that it will fuse. Its helium product, deposited close to the core, will also burn. This state, in which several fusion processes take place around the core, along with a single process throughout the core itself, is known as *shell burning*, and is illustrated in Figure 2.

As seen in the diagram, successive products undergo fusion themselves until iron is produced through silicon-burning. Iron-burning is an endothermic reaction, so its formation signals imminent core collapse. Unlike lower mass stars, gravity is able to overcome electron degeneracy pressure and collapse continues until the formation of a degenerate neutron state. At this point, the core is stable but the outer layers (where shell burning had been taking place) are continuing to fall. The innermost layers bounce off the core, sending an explosive shock outward which contributes to ripping apart all of the former star but its core (an incredible outflow of neutrinos from the col-
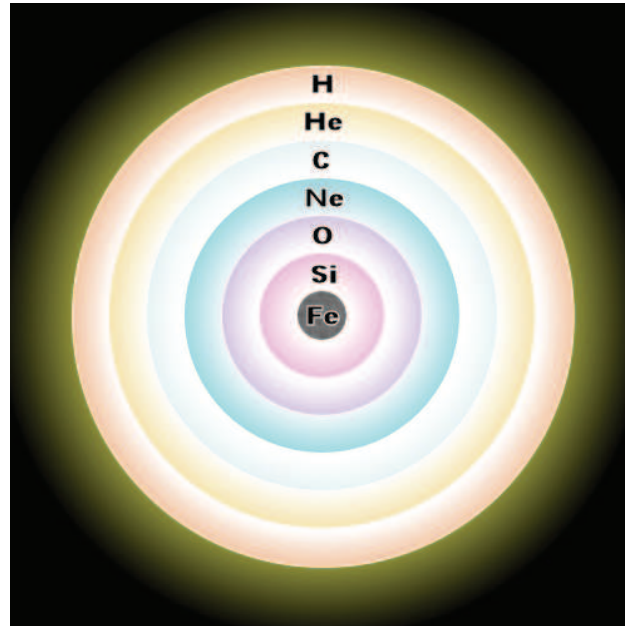
Figure 2: Dying massive stars undergo a single fusion process throughout their core, along with layers of shell burning around the core where abundances and temperatures are sufficient. Once a particular fuel is exhausted in the core, it will begin to burn in a shell, and its product will begin burning throughout the core. This continues until the production of iron. As the fusion of iron absorbs energy, rather than releasing it, the star as illustrated is on the brink of core collapse. Diagram not to scale. By: R. J. Hall, released under CC Attribution 2.5 license.

lapsed core is also responsible for much of the destruction). The aftermath of a Type II supernova sees the formation of a neutron star and a surrounding nebula of processed gases and light metals.

The most massive main-sequence stars ($> 11 M_\odot$) almost certainly undergo supernova with an iron core. The fates of 8 - 11 $M_\odot$ stars, such as the progenitor of the Crab pulsar, are less well known. It is possible that they also attained an iron core, though studies have shown that a degenerate oxygen-neon-magnesium core is also possible (Nomoto 1985). The surface of the resultant neutron star, however, would still contain neutron-rich nickel and iron-peak nuclei due to the existence of the neutron superfluid just below the crust (discussed below).

1.2   The "Discovery" of Neutron Stars

In 1933, Walter Baade and Fritz Zwicky proposed that some supernovae resulted in the formation of neutron stars. This is particularly remarkable as Chadwick had discovered the neutron only a year prior. Baade & Zwicky had been working on an explanation for the origin of supernovae. A number of years passed and great strides were made in the theoretical understanding of neutron stars. Theories were proposed as to their internal structure, surface characteristics, magnetospheric properties and so forth. This represented excellent foundational work, but there was little indication that neutron stars actually existed.

Then, in 1967, Jocelyn Bell Burnell, under the direction of Anthony Hewish, observed a hand-

Zone	Density	Thickness	Temperature
Atmosphere	10^2	10 cm	?
Plasma Envelope	10^{10}	100 km	$\sim 10^6$ K
Crust (Crystalline Lattice)	4×10^{11}		$\sim 10^6$ K
Crust (Solid with Free Electrons)	10^{14}	1 km	
Neutron Superfluid	2×10^{15}	9 km	10^8 K
Core	3×10^{15}		$10^8 - 10^{10}$ K

Table 1: Parameters for the interior of "typical" neutron star. The units of density are g/cc. Data compiled from Ginzburg (1971), Kaspi et al. (2006), and Lyne & Graham-Smith (2006).

ful of objects that emitted radio signals that disappeared and reappeared at regular intervals. They named the objects *pulsars* (due to the radio pulses they produce) and work commenced on explaining their origin. Researchers came to realize that pulsars are, in fact, rapidly rotating, active neutron stars. Active neutron stars have immensely powerful magnetic fields, which beam photons and particles outward from the magnetic poles. The magnetic poles are not necessarily aligned with the rotational axis, causing a *lighthouse effect* in which the beam sweeps across an observer's field of view.

The connection between pulsars and neutron stars allowed for the verification of many theoretical neutron star properties. A model for the "typical" neutron star emerged and is illustrated in Table 1.

In many ways, a neutron star can be thought of as a single, massive neutron in space. The composition of its core is currently unknown, owing to its immense density, though suggestions have been made that it consists of a pion condensate or a quark superfluid. The bulk of the object (9 km out of a typical 10 km radius) exists as a hot, roughly isothermal, degenerate neutron superfluid. Though the object was once composed of iron nuclei and electrons, the temperatures and densities achieved upon core collapse eventually force the protons and electrons to merge, forming neutrons. It is not until the outer 1 km that electrons and protons are free to exist, though the electrons generally form a degenerate state. This area is known as the crust, the uppermost layer of which is primarily a crystalline lattice of iron-peak nuclei, surrounded by a "sea of electrons," and studded with heavier nuclei formed through spallation processes (Jones 1977). This state is discussed in great detail at the beginning of Section 4. As examined in Section 2, Michel (1975) argues that a thin layer of helium may exist on top of the iron lattice.

The next two zones exist separately from the rest of the neutron star, and are the subject of much debate in the literature. Their values in Table 1 represent a compromise situation of sorts. A relatively small vacuum exists between the crust and the plasma envelope, as enunciated in the Ruderman & Sutherland model (see Section 3). In this model, the plasma envelope is in a state of constant flux, being fed by electrons leaving the surface of the neutron star, as well as positrons formed in the vacuum gap. These particles are later ejected into the surrounding nebula. Before their departure from the neutron star environment, the particles pass through a thin, relatively rarefied atmosphere. Our areas of interest for this investigation are the crystalline lattice and the lower portions of the plasma envelope.

1.3   Specific Properties of the Crab Pulsar

We now realize that a Type II supernova may result in the formation of a pulsar surrounded by a gaseous nebula. The pulsar is a highly energetic, rapidly rotating neutron star, which enables it to, for instance, illuminate its companion nebula through synchrotron radiation. This is beautifully illustrated by the Crab Nebula (Figure 1). The following list collects the various parameters of the Crab Pulsar that we will use in all calculations for this investigation.

- **Neutron Star Radius:** In the typical neutron star, **1.4** $M_\odot$ of material occupies a sphere of radius 10 - 20 km. The Crab is estimated to have a radius of **15.6 km** (Kaspi et al. 2006).

- **Neutron Star Rotational Period:** As stated above, pulsars are powered by rapidly rotating neutron stars. Their velocity is due to conservation of angular momentum from the progenitor star. The period of the Crab pulsar has been determined to be **33 ms** (Kaspi et al. 2006).

- **Pulsar Magnetic Field:** The literature aptly describes the magnetic fields found in the vicinity of a neutron star as *superstrong*. As with angular momentum, the progenitor star's magnetic flux is also conserved, leading to an exponentially more intense field on the much, much smaller neutron star. The strength typically ranges from $(1 - 5) \times 10^8$ tesla. We will use 2×10^8 **T** (2×10^{12} **gauss**) for the Crab pulsar (Kaspi et al. 2006).

- **Field Line Distortion:** There is an area of the magnetosphere surrounding a neutron star that corotates with the object. This is known as the *light cylinder*. Magnetic field lines which originate in the polar cap region become distorted as they cross the light cylinder. This distortion must be corrected for when calculating the area of the polar cap, accomplished through the use of the constant κ. We will use the standard value, $\kappa = (\frac{2}{3})^{(3/2)}\pi$ (Ruderman & Sutherland 1975).

- **Gap Particle Acceleration:** Under the Ruderman & Sutherland pulsar model (Section 3), a very large potential develops across a gap that forms between the neutron star surface and the magnetosphere above the magnetic poles. If we use an approximation adapted from Ruderman & Sutherland (1975), $\Delta V \approx 1.2 \times 10^{11} B^{-1/7} P^{-1/7} \rho^{4/7}$ (ρ defined by equation (22)), the voltage is roughly $\Delta V = 1.1 \times 10^{13}$ **volts**. Particles in the gap are accelerated to ultrarelativistic speeds, reaching Lorentz factor $\gamma = 2.2 \times 10^7$.

2   The Helium Problem

The majority of the roughly 2 $M_\odot$ comprising the Crab Nebula is helium. For the most part, it is well understood as mantle material ejected during the supernova event. There is, however, a torus containing ~ 0.5 $M_\odot$, 95% of which is helium, that stretches across the pulsar region and has not been given a satisfactory explanation (MacAlpine et al. 2007). The question arises whether the torus has been built over the 1000 years since the supernova by helium leaving the surface of the neutron star located at the center of the nebula.

To a first-order approximation, the outer surface of a neutron star is modeled as a crystalline lattice of iron-peak nuclei (De Blasio & Lazzari 1996). Under the standard model (Section 3), the electric fields that develop in the surrounding magnetosphere are unable to lift these heavy

positive ions from the surface; only the much less bound electrons will escape. F. C. Michel (1975), however, was interested in developing a model for the pulsar magnetosphere that was driven by positive ions. He reasoned that if Fe ions were too strongly bound, there might be a sufficient amount of helium present on the surface to power his model. Based on calculations presented in Section 4, helium ions on the surface of a neutron star would have roughly 3% the binding energy of iron nuclei, owing to their much lower charge number. Helium ions are therefore considered to be as free as electrons. The following argument is presented in Michel (1975):

Assume that there are some quantities of positive ions (like helium) on the surface of a neutron star, and that they are freely able to escape into the surrounding space. Their departure produces a torque on the neutron star, stealing some rotational energy (and causing the object to slow by a small amount). We relate the number of ions leaving the surface, N, to the angular velocity, ω:

$$N = \int_{\omega_o}^{\omega} \frac{\dot{N}}{\dot{\omega}} d\omega. \tag{1}$$

As ions leave the surface, they build up in the area immediately above the surface, accumulating a *space charge density*, ρ_S, given by:

$$\rho_S = 2\epsilon_o \, \boldsymbol{\omega} \cdot \mathbf{B}. \tag{2}$$

This ion cloud limits the number of ions which can leave through the polar cap region, which has an area of:

$$A = \frac{\kappa \omega R^3}{c}, \tag{3}$$

where κ is a correction for field line distortion away from the surface and R is the radius of the neutron star. If we multiply equations (2) & (3) together, along with c, we can find the *space-charge limited current* produced by the departing ions:

$$I = (2\epsilon_o \, \boldsymbol{\omega} \cdot \mathbf{B}) \frac{\kappa \omega R^3}{c} c \tag{4}$$

$$= -2\kappa \epsilon_o R^3 B \omega^2. \tag{5}$$

This assumes that $\boldsymbol{\omega}$ is anti-parallel to $\boldsymbol{B}$, following the definition for a pulsar given in section 3. Dividing this current by the charge per escaping ion, Ze, we can determine the ion number loss rate, $\dot{N}$:

$$\dot{N} = -\frac{2\kappa \epsilon_o R^3 B}{Ze} \omega^2. \tag{6}$$

The angular acceleration, $\dot{\omega}$, is simply the torque caused by the mass loss divided by the neutron star's moment of inertia, $\mathscr{I}$:

$$\dot{\omega} = \frac{2\pi \kappa^2 (R^3 B)^2}{\mu_o c^3 \mathscr{I}} \omega^3. \tag{7}$$

Using equations (6) & (7) in equation (1), and evaluating the integral, we find:

$$N = \left(\frac{c}{e\pi\kappa}\right) \frac{\mathscr{I}}{ZR^3 B} \ln\left(\frac{\omega}{\omega_o}\right). \tag{8}$$

As we have basically just solved a growth equation, the quantity multiplying $\ln\left(\frac{\omega}{\omega_o}\right)$ is the number of ions initially present on the surface, N_o. Michel (1975) went on to establish the "helium budget"

for the average neutron star, concluding that the initial amounts available, as well as the modest loss rates, indicated that neutron stars could retain surface helium for "considerable lengths of time."

Using the standard values for the Crab Pulsar (Section 1.3, page 5), we determine that:

$$N_o = \frac{1.25 \times 10^{44}}{Z} \text{ ions,} \tag{9}$$

or, 4.16×10^{17} kg of ionized helium were present on its surface when the neutron star was born. *As such, the surface of the neutron star cannot be considered a source for roughly 10^{30} kg of helium orbiting the pulsar in the yet-unexplained torus.*

3 The Pulsar Model

Michel's (1975) approach to the neutron star surface composition, utilized in Section 2, did not require a fully enunciated electrodynamical model of surface and magnetosphere physics. It was based only on the assumptions that charges were present on the surface, and that these charges could freely leave said surface. Though they may not accurately reflect the reality of the situation, these assumptions still allowed us to determine a maximum amount of ionized helium present on a neutron star armed only with the knowledge of its mass, radius and magnetic field strength. If anything, the assumptions are far too generous and likely overestimate the amount of the helium available; still, our calculated value was some 12 orders of magnitude less than the amount observed in the torus we sought to explain. Correcting the assumptions would require introducing some binding to the surface of the helium (the ions are no longer free) and an accurate knowledge of the forces removing the ions. These would increase the difficulty of removing helium and drive the "initial" amount of helium, N_o, down.

Though a more rigorous analysis was not necessary in the case of helium, it will now be required for investigating the problem of anomalous nickel observed in the Nebula. In looking to the surface as a possible source, we must certainly take into account the degree to which the nuclei are bound to the surface, as well as the processes that could supply the energy needed to break the ions free. For this, we require a developed model of the pulsar near-surface magnetosphere, and have turned to the landmark paper produced by M. A. Ruderman & P. G. Sutherland in 1975.

3.1 Charge Separation in the Magnetosphere

Once again, we imagine that a pulsar is a neutron star which is rapidly rotating with an extremely strong magnetic field. The characteristics of the corotating magnetosphere were first advanced by Goldreich and Julian (1969). For now, we assume that the surface contains a collection of both positive and negative charges, free to move about the surface. The field lines for the magnetic field penetrate the surface; that is, the charges are able to "interact" directly with the lines. We describe the electromagnetic field of the magnetosphere, from an observer's frame, in the traditional way:

$$\mathbf{E} = -(\mathbf{\Omega} \times \mathbf{r}) \times \mathbf{B}, \tag{10}$$

where Ω is the angular frequency of the magnetosphere at a distance r from the neutron star center. For distances r less than R_c the magnetosphere perfectly rotates with the neutron star. R_c is a radius
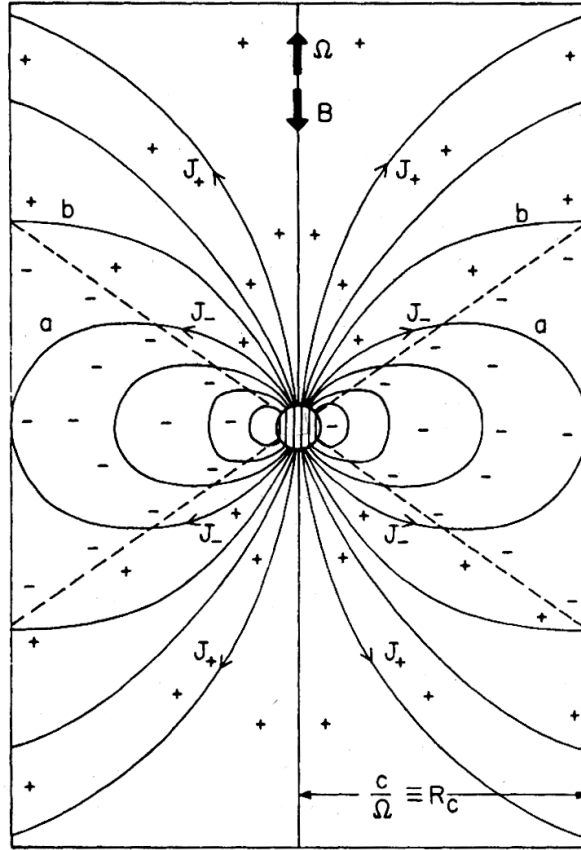
Figure 3: Sketch of the Goldreich & Julian model for the light cylinder about a neutron star. Line (a) is the last closed field line within the light cylinder, allowing for particles to return to the surface of the neutron star. Particles traveling along lines from (b) to the polar cap may leave the region, as these lines are considered "open." Image from Ruderman & Sutherland (1975).

that delimits an area known as the *light cylinder* and is defined:

$$R_c \equiv \frac{c}{\Omega} \, . \tag{11}$$

Roughly, space inside the light cylinder outpaces that outside, and so magnetic field lines are "broken" as they emerge from the light cylinder. These are interpreted as open field lines, and particles moving along them can exit the light cylinder, leaving the lower magnetosphere. It is these lines, schematically represented as (b) and those above it in Figure 3, that are responsible for the jets observed in Figure 1.

Charged particles are contained in the equatorial region but are allowed to leave through the polar cap of the light cylinder, creating regions of separated positive and negative charge in the magnetosphere. Their locations, either equatorial or polar, depend on the state of symmetry between the rotation and magnetic axes. Antisymmetry leads to a positive polar magnetosphere, as seen in Figure 3, and Ruderman & Sutherland declare this arrangement a *pulsar*. Its opposite, resulting in a negative polar magnetosphere, is termed an *antipulsar*.

8

Charge separation in the magnetosphere causes a potential difference to form between the polar cap and the equator on the surface of the neutron star. This potential difference induces the motion of charged particles beneath the stellar surface. Interactions between these currents and the magnetic field lines piercing the surface introduce a braking torque. Ruderman & Sutherland (1975) find that the rotational energy lost through this torquing is ultimately manifested in the acceleration of particles along the "open" field lines. The energies tapped are extremely small as compared to the rotational kinetic energy of the neutron star, but are sufficient to accelerate charged particles to ultrarelativistic speeds, with Lorentz factors upwards of $\gamma = 10^7$.

3.2   Separation of the Polar Magnetosphere from the Surface

Goldreich & Julian force the constraint on their model that the magnetosphere must maintain $\mathbf{E} \cdot \mathbf{B} = 0$. Deviations from zero are met with the necessary number of particles, supplied from the surface, to return to this constraint. There is no preference for positively- or negatively-charged particles. This is similar to the assumptions made above for Michel's work; "free" positively- and negatively-charged particles are assumed to exist. On the surface of an actual neutron star, however, positive charges are predominately found in the form of iron-peak nuclei (Ruderman 1971). These heavy ions are much more difficult to remove from the surface than electrons due to the relatively high binding energy of the iron lattice (as discussed in Section 4). Ruderman & Sutherland (1975) exhaustively show that the typical neutron star is incapable of releasing iron-peak nuclei from its surface, while electrons, requiring at least an order of magnitude less energy, are readily expelled along "open" field lines.

Positive charges already in the polar magnetosphere (for whatever reason) continue to flow out of the light cylinder along "open" field lines. Without a ready supply of replacements from the surface, the magnetosphere actually shrinks away and a region forms where $\mathbf{E} \cdot \mathbf{B} \neq 0$. This is known as a *gap*, though the more frequent term when working with pulsars is *polar gap*. The electric field at the bottom of the polar gap (the polar surface of the neutron star), is given by:

$$E_p = 2\Omega B h, \tag{12}$$

where h is the gap width. To simplify the math, the magnetosphere is assumed to be free of currents, so that the electric field vanishes at the top of the gap. This allows us to determine the potential difference across the gap:

$$\Delta V = \Omega B h^2. \tag{13}$$

We may now fully appreciate the ability of a neutron star to accelerate particles. The "gap voltage" for the Crab Pulsar is roughly 10^{13} V; electrons accelerated through the gap gain $10\,\text{TeV}$ of kinetic energy! This corresponds to a γ value of approximately 2×10^7.

3.3   Pair Creation in the Polar Gap

Photons can react with matter either through the photoelectric effect, Compton scattering, or pair production, depending on the amount of energy they contain. Photons with sufficiently high energies ($\geq 2m_e c^2$), in the presence of a massive particle, can spontaneously decay into an electron-positron pair. The massive particle is required for momentum conservation, as the e^+/e^- pair travel directly away from one another. A sufficiently strong magnetic field, however, can also absorb this
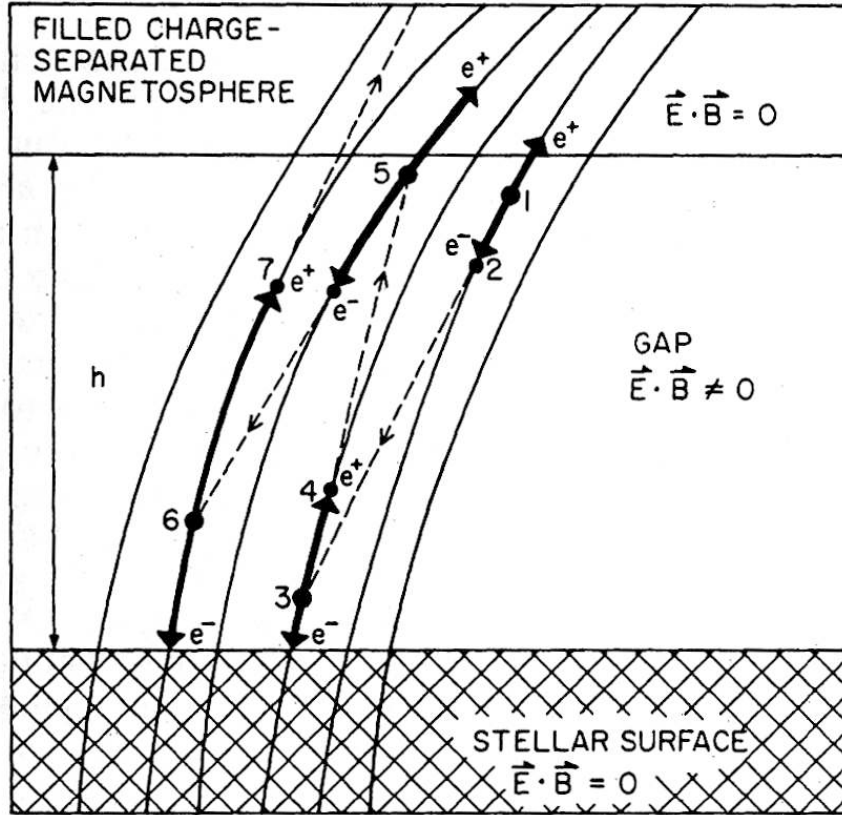
Figure 4: The development of a pair avalanche in the polar gap of a pulsar. The conversion of surface-radiated photons triggers a chain reaction of pairs producing synchrotron radiation which go on to form additional pairs. Image from Ruderman & Sutherland (1975).

momentum kick, and so may be substituted for the massive particle. Such a field is readily found in the polar gap of a pulsar, where the conversion rates for γ-rays run as high as 10^5 s^{-1} (Ruderman & Sutherland 1975).

The newly-formed gap pairs are rapidly accelerated to the ultrarelativistic Lorentz factors discussed above, allowing them to release profuse amounts of photons through curvature radiation. This is a distinct process from synchrotron radiation, and is due to the fact that the pairs move along curved magnetic field lines, thereby being subject to centripetal acceleration. Their motions along these field lines may develop a spiral, which would generate synchrotron radiation; this possibility is investigated in Section 5. The curvature photons are utilized for further pair production, and a e^+/e^- avalanche (Figure 4) ensues.

The pairs are formed parallel to the magnetic field lines, and instantaneously separated. The electrons are drawn toward the positively-charged polar surface in a great cascade. The positrons move into the withdrawn magnetosphere. Now replenished, it reconnects with the surface and the polar gap momentarily vanishes. Of course, positrons are still exiting the magnetosphere through the light cylinder, and so the polar gap begins to reform.

The vacuum gap h must be wide enough that the production of e^+/e^- pairs is significantly likely. The mean free path of a photon in a magnetic field is (Erber 1966):

$$l \approx \frac{n_{pairs}}{n_{photons}} \alpha(\chi)^{-1}. \tag{14}$$

$\alpha(\chi)$ is a coefficient of photon attenuation, which has a value determined by:

$$\alpha(\chi) = \frac{1}{2} \frac{\alpha}{\lambda_e} \frac{B_\perp}{B_q} T(\chi), \tag{15}$$

where α is the fine structure constant:

$$\alpha = \frac{e^2}{4\pi\epsilon_o \hbar c}, \tag{16}$$

and λ_e is the reduced de Broglie wavelength for an electron (Ruderman & Sutherland 1975):

$$\lambda_e \approx \frac{\hbar}{m_e c}. \tag{17}$$

$\frac{B_\perp}{B_q}$ is the ratio of two magnetic fields. The first is the actual magnetic field influencing the photon (Ruderman & Sutherland 1975):

$$B_\perp = B \sin\theta \approx \frac{l}{\rho} B, \tag{18}$$

where ρ is defined below in equation (22) and θ is the pitch angle between the photon's velocity and the magnetic field line. The second magnetic field of concern is a constant quantum mechanical magnetic field (Erber 1966):

$$B_q = \frac{m_e^2 c^2}{e\hbar}. \tag{19}$$

Finally, $T(\chi)$ is a function that depends on the value of χ, the cross-section for photon conversion in a strong magnetic field (Erber 1966):

$$\chi \equiv \frac{1}{2} \frac{\hbar\omega}{m_e c^2} \frac{B_\perp}{B_q}, \tag{20}$$

where $\hbar\omega$ is the energy of the converted photons (Ruderman & Sutherland 1975):

$$\hbar\omega \approx \frac{3}{2} \gamma^3 \frac{\hbar c}{\rho}, \tag{21}$$

ρ being the radius of curvature of the magnetic field lines near the neutron star surface (Ruderman & Sutherland 1975):

$$\rho \approx \sqrt{\frac{Rc}{\Omega}} = 1.6 \times 10^5 \text{m}, \tag{22}$$

using standard values (page 5). We expect χ to be small (Ruderman & Sutherland 1975), so we use (Erber 1966):

$$T(\chi) = 0.46 \exp\left(-\frac{4}{3\chi}\right), \tag{23}$$

11

in equation (15). Altogether, using equations (16) through (23) in equation (15) we find:

$$\alpha(\chi) = \frac{1}{2}\frac{e^2}{4\pi\epsilon_o \hbar c}\frac{m_e c}{\hbar}\frac{l}{\rho}B\frac{e\hbar}{m_e^2 c^2}\left[0.46\exp\left(-\frac{4}{3\chi}\right)\right] \tag{24}$$

$$= \frac{23}{400}\frac{e^3}{\pi\epsilon_o \hbar m_e c^2}\frac{l}{\rho}B\exp\left(-\frac{4}{3\chi}\right). \tag{25}$$

Now, from equations (20) and (21):

$$-\frac{4}{3\chi} = -\frac{16}{9}\frac{(m_e c)^3}{e\hbar^2}\frac{\rho^2}{\gamma^3 B}\frac{1}{l}, \tag{26}$$

$$\text{let}\quad \delta = -\frac{16}{9}\frac{(m_e c)^3}{e\hbar^2}\frac{\rho^2}{\gamma^3 B}, \tag{27}$$

which, when used in equation (25), gives us a final form of the photon attenuation coefficient $\alpha(\chi)$:

$$\alpha(\chi) = \frac{23}{400}\frac{e^3}{\pi\epsilon_o \hbar m_e c^2}\frac{l}{\rho}B\exp\left(\frac{\delta}{l}\right), \tag{28}$$

$$\alpha(\chi)^{-1} = \frac{400}{23}\frac{\pi\epsilon_o \hbar m_e c^2}{e^3}\frac{\rho}{Bl}\exp\left(-\frac{\delta}{l}\right). \tag{29}$$

Combining equation (29) with equation (14), we have an expression for the mean free path length of a photon in a magnetic field:

$$l^2 = \frac{n_{pairs}}{n_{photons}}\frac{400}{23}\frac{\pi\epsilon_o \hbar m_e c^2}{e^3}\frac{\rho}{B}\exp\left(-\frac{\delta}{l}\right). \tag{30}$$

In the limit of quasi-steady discharge, there is a one-to-one correspondence between photons and e^+/e^- pairs; that is, $n_{pairs} = n_{photons}$ (Ruderman & Sutherland 1975). The mean free path for a photon is then the total gap width, h. Using this approach, along with the standard values for the Crab Pulsar, we find that the polar gap has a quasi-steady thickness of 11.57 meters.

3.4   Summary of Model

We have now assembled a workable model for the set of pulsar physics relevant to our problem. A pulsar is a neutron star which rapidly rotates with an incredibly strong magnetic field. The magnetosphere is only capable of corotating with the neutron star out to a certain distance, which defines the light cylinder. The field outside of the light cylinder lags behind the field inside, causing a break in the magnetic field in the polar region. The polar magnetic field lines are now considered "open," allowing them to transport charged particles away from the surface of the neutron star and into the surrounding space.

The presence of "open" and closed field lines within the light cylinder causes the polar and equatorial regions of the magnetosphere to fill with differently-charged particles (i.e., in a *pulsar*, the polar magnetosphere, within the light cylinder, is primarily filled with positrons). This charge separation allows the pulsar to function as a tevatron-scale particle accelerator.

Typical pulsars are incapable of lifting positive ions from the surface of their neutron star. As the polar magnetosphere is continually ejecting positrons away from the neutron star and cannot

be replenished by the surface, it shrinks away from the surface. The combination of the ensuing vacuum gap and the superstrong magnetic field, along with γ-rays from the surface, results in the prodigious creation of e^+/e^- pairs. The pairs separate, with the positrons refilling the polar magnetosphere while the electrons flood the surface. We assume that this is all accomplished quasi-steadily, such that there is a near-continuous flux of electrons toward the surface.

3.5 Application of the Model to the Crab Pulsar

The goal of this paper is to examine the possible use of the neutron star surface to explain the origin of anomalous regions of ions (primarily helium, already discussed, and nickel) in the Crab Nebula. The pulsar model that has been presented as the basis of our work on this problem does not support ions leaving the surface of the neutron star, in general. However, Ruderman & Sutherland acknowledge that, in the specific case of the Crab Pulsar, it may be young and energetic enough to "boil ions off of the surface" (1975). We have interpreted this to mean that the Crab pulsar is capable of thermionic emission of positive ions from its surface. Though it is possible that this will effect the full development of the polar gap, we hold the assumption that the amount of positive ions removed is dwarfed by the number of positrons flowing out from the light cylinder. In this way, the gap condition $\mathbf{E} \cdot \mathbf{B} \neq 0$ holds and the model is, for the most part, intact. We will return to these possible concerns later, after we have fully enunciated the mechanisms by which positive ions may be removed from the surface.

4 Iron-Peak Nuclei Bound to the Surface

The possibility for iron-peak nuclei to leave the surface of a neutron star is dependent on two things: the amount of energy binding the ions to the surface, and the availability of processes to supply this energy. Below, we present the variational procedure used to calculate the binding energy of iron nuclei in the presence of a super-strong magnetic field, and also consider three possible sources that could supply this work function: residual thermal energy from the supernova, Ohmic heating caused by subsurface currents, and heating through irradiation of the surface by polar gap electrons.

We have already seen an example of the extreme physics associated with super-strong magnetic fields in the high probability of photon conversion in the polar gap. Matter is also significantly affected by the intense fields: the Lorentz force is stronger than even the atomic scale Coulomb interaction between electron and nucleus, and the electrons are forced to occupy cylindrical Landau orbitals (Cohen-Tannoudji 1977). Interestingly, in the field present on the surface of the Crab Pulsar, the zeroth Landau orbital:

$$\rho_0 = \sqrt{\frac{3\hbar}{eB}} = 3.14 \times 10^{-12} \text{ m}, \tag{31}$$

is actually less than the Bohr radius $a_o = 5.29 \times 10^{-11}$ m. Nuclei and electrons in a field of this intensity will exist as either individual, multi-electron atoms or as condensed matter, favoring the phase with the lowest ground state energy.

4.1 Energy for Individual Atoms

Flowers et al. (1977) present variational calculations for the binding energies of iron in the relevant phases. First, they calculate the binding energy for free atoms, utilizing the Hartree-Fock method for calculating the wave functions of many-electron atoms as the antisymmetrized product of single-particle wave functions. This results in the total wave function, in cylindrical coordinates:

$$\psi(r_1, \ldots, r_z) = A \prod_{i=1}^{Z} R_{m_i}(\rho, \phi) f_{v_i}(z), \tag{32}$$

where i steps through the number of electrons, each of which will have an associated quantum numbers m and v. The radial function $R_m(\rho, \phi)$ is described by:

$$R_m(\rho, \phi) = \left[2\pi(m!)\hat{\rho}^2\right]^{-\frac{1}{2}} e^{-im\phi} \left(\frac{\rho^2}{4\hat{\rho}^2}\right)^{\frac{m}{2}} \exp\left(-\frac{\rho^2}{4\hat{\rho}^2}\right), \tag{33}$$

where ρ is, again, the Landau orbital:

$$\rho_m = (2m + 1)^{\frac{1}{2}}\hat{\rho} \tag{34}$$

$$\hat{\rho} = \left(\frac{\hbar}{eB}\right)^{\frac{1}{2}}. \tag{35}$$

The quantum number m may be any positive integer (or zero). The other function $f_v(z)$ depends on the number of nodes in the wave function, of which we only consider $v = 0$ and $v = 1$. The z-dependence is approximated using exponentials:

$$f_0(z) = (\alpha)^{\frac{1}{2}} e^{-\alpha|z|} \tag{36}$$

$$f_1(z) = (2\alpha)^{\frac{3}{2}} z e^{-\alpha|z|}. \tag{37}$$

Thus, every orbital m has two variational parameters, α and v.

Now that we are in possession of a fully described wave function, we may determine the energy function, which has four terms: kinetic K, electron-nucleus potential V_{en}, direct electron-electron potential V_{ee}^{dir}, and exchange electron-electron potential V_{ee}^{ex}. Each term, except for the straightforward kinetic energy, contains a number of highly complicated integrals equal to the number of electrons belonging to the atom, each of which must be evaluated numerically and then minimized by varying the quantum parameters. We did not carry out these calculations. Flowers et al. (1977) discovered that some electrons in the one-node state must be used to minimize the energy profile, and their minimum values for the binding energy are collected in the first row of Table 2, page 16.

4.2 Energy for Condensed Matter

We must now determine the binding energy of the iron if it exists as condensed matter. The calculation is begun by considering the situation in which "point-nuclei" are arranged in a body-centered cubic lattice, immersed in a uniform sea of electrons. The lattice is then divided into electrically neutral spherical shells, such that the energy per cell is only radially dependent. This

14

allows for a straightforward minimization, resulting in the following expression for energy per lattice cell (Flowers et al. 1977):

$$E = -42.63 \, B_{12}{}^{2/5} \left(\frac{Z}{26}\right)^{9/5} \text{keV}, \tag{38}$$

where B_{12} is the magnetic field strength in units of 10^{12} gauss. Since the energy only depends on cell radius, we also know the optimal spacing of nuclei in the lattice:

$$a = 0.648 \left(\frac{\pi}{3}\right)^{\frac{1}{3}} a_o \left(\frac{Z}{26}\right)^{\frac{1}{5}} B_{12}^{-\frac{2}{5}} \text{cm}, \tag{39}$$

where a_o is the Bohr radius. We find that a lattice on the surface of the Crab Pulsar will have a spacing of $a = 2.64 \times 10^{-11}$ m and a binding energy per nucleus of $E = -56.25$ keV. This is more positive than the value found for individual atoms in a similar strength magnetic field (Table 2), suggesting that iron exists in an unbound state on the Crab Pulsar surface. However, additional cohesive binding is provided in two ways: nonuniform electron distribution and the formation of "ion cores."

Regarding the former, the calculations to this point have assumed that the ion lattice is easily divisible into spheres of one iron nucleus and 26 uniformly distributed electrons. In fact, the electrons are magnetically confined to move in cylindrical spaces, and further energy reductions may be gained through the nonuniform distribution of electrons in these Landau orbitals. We imagine that the lattice cells now resemble tapered cylinders, and the entire arrangement appears as linear chains of ions. The electrons are still considered to constitute a "sea," but their movement is now somewhat more restricted. With these constraints, Flowers et al. (1977) performed new variational calculations, the results of which are recorded in the second row of Table 2. We note that a condensation of nuclei, grouped in linear chains, is now the energetically favorable phase.

4.3   The Cohesive Energy

The differences between the ground state energies of ion-electron structures in these two phases (free atoms versus linear chains) is known as the *cohesive energy* ΔE (Flowers et al. 1977). We have found that the surface of the neutron star in the Crab Pulsar is likely covered with a tightly bound lattice of iron nuclei. Its existence as the favored phase of matter is one of the main arguments that Ruderman & Sutherland make against the removal of positive ions from the surface. However, we know that, if the difference in energies between bound and unbound matter, the cohesive energy, is provided to a nucleus in the lattice, it will become unstuck. In this way, the cohesive energy is also the *work function* for lattice-bound positive ions (Jones 1978). An unstuck ion is easily lifted by the surface electric fields (Ruderman & Sutherland 1975), as the sufficient energy to remove it from the lattice binding it to the surface has been provided. The additional binding energy, for example 63.21 keV in the case of 2×10^{12} gauss fields, is the total energy holding the free, individual "atom" together. Its provision in not necessary for the spontaneous emission of positive ions from the neutron star surface.

There is one last correction that must be made, mentioned above as the formation of "ion cores." We saw how the binding energy in the lattice was reduced by roughly 10 keV when the electrons were confined to tapered cylinders. Slight additional gains in binding energy may be had

Binding Energy Profile for Iron in Super-strong Magnetic Fields

	Magnetic Field (10^{12} gauss)				
	1	2	3	4	5
Individual Free Ions					
$-E_{free}$	48.48	63.21	73.69	82.08	89.43
Linear Ionic Chains					
$-E_{chain}$	50.24	66.32	78.05	87.53	95.74
Cohesive Energies					
ΔE	1.76	3.11	4.36	5.45	6.31
$\Delta E'$	2.6	4.1	5.4	6.8	8.0

Table 2: Binding energies for the two possible phases of iron matter under the influence of super-strong magnetic fields found on a neutron star surface. The difference between these is the cohesive energy ΔE, which is also the work function for removing nuclei from the energetically favored lattice phase, allowing them to leave the surface. Small corrections to the lattice calculation produce the true work function, $\Delta E'$. Data reprinted from Flowers et al. (1977).

if some electrons are removed from the sea and closely bound to a single nucleus. In this way, the electrons now fall into two classes: free conduction electrons and bound core electrons. The last row of Table 2 contains the final cohesive energies (Flowers et al. 1977), synonymous with the work functions for removing iron nuclei from the surface. The cohesive energy has no temperature dependence - condensation is purely the result of the intense surface magnetic fields, forcing the individual atoms close enough that they prefer to exist as a lattice. Thus, we can express the work function as a simple function of B:

$$U = \Delta E' = 2.6 B_{12}^{0.7} \text{ keV}, \tag{40}$$

as suggested by Jones (1978) and illustrated in Figure 5. The most probable mechanism for providing this amount of energy, and thus breaking ions loose from the lattice, is the ambient surface temperature of the neutron star. Ions freed from the lattice are no longer bound to the surface and are freely emitted into the surrounding space along the magnetic field lines exiting the polar cap area through the light cylinder. This is the thermionic emission of iron ions investigated by Jones (1978). He provides approximate expressions for the number rate of ion loss from the surface:

$$\Gamma = \frac{U}{ha^2} e^{-(\beta U)} \text{ ions/s/m}^2, \tag{41}$$

$$\beta = \frac{1}{k_B T}. \tag{42}$$

Recall that equation (40) gives U in keV, so the appropriate h (here Planck's constant) and k_B (Boltzmann constant) must be used; a is the lattice constant, equation (39), which is used in meters so that Γ has dimensionality ions/s/m^2. Figure 6 plots the iron loss rates (in kg/s) from the polar cap region of the Crab pulsar as a function of both temperature and magnetic field strength. The polar cap area is given by equation (3). Figure 6 illustrates the significant gains that are made in emissions as the temperature of the polar cap increases from 1×10^6 K to 4×10^6 K. In order to
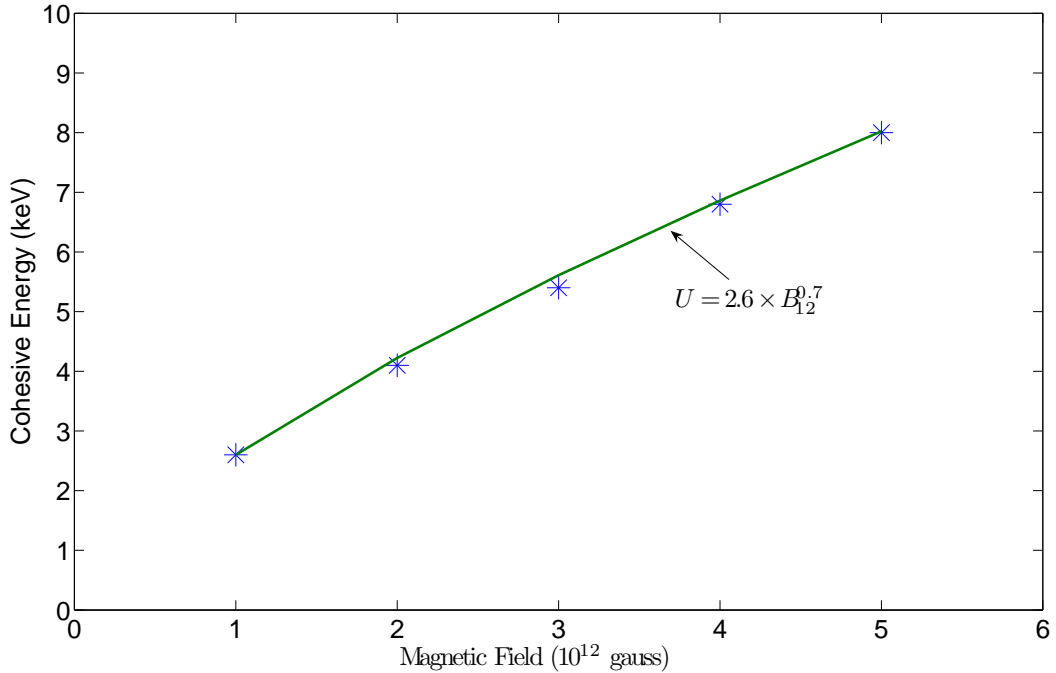
Figure 5: This plots the cohesive energy for iron (stars) as a function of magnetic field strength in units of 10^{12} gauss. The line fits the data according to the equation shown, which comes at the suggestion of Jones (1978).

assess the rate at which the Crab pulsar emits positive ions, we now endeavor to determine the residual surface temperature of the Crab Pulsar and investigate the possible mechanisms that could further heat portions of its surface. The presence of significant heating over its lifetime would dramatically increase the amount of iron-peak nuclei able to be sent into the surrounding nebula.

5 The Removal of Positive Ions

5.1 Base Surface Temperature of the Crab Pulsar

Neutron stars produced by the most massive main-sequence stars previously existed as an iron core, immediately prior to the onset of a supernova event. The iron is a product of silicon-burning, which requires temperatures in excess of 2.7×10^9 K to take place. As previously mentioned, main-sequence stars in the range of 8-11 $M_\odot$ may only be able to form an oxygen-neon-magnesium core (Nomoto 1985). These elements are the products of carbon burning, which requires temperatures in excess of 6×10^8 K. In the course of the supernova, a great deal of thermal energy is used in photodisintegration or is carried away from the core through neutrino emissions (Protheroe et al. 1998), such that the surface of the neutron star in the first $\sim$10 years of its existence is generally given as $(4 - 5) \times 10^6$ K (Tsuruta et al. 1972, Van Riper 1991). From this point onward, cooling is primarily accomplished through photon emissions from the surface, which is warmed via
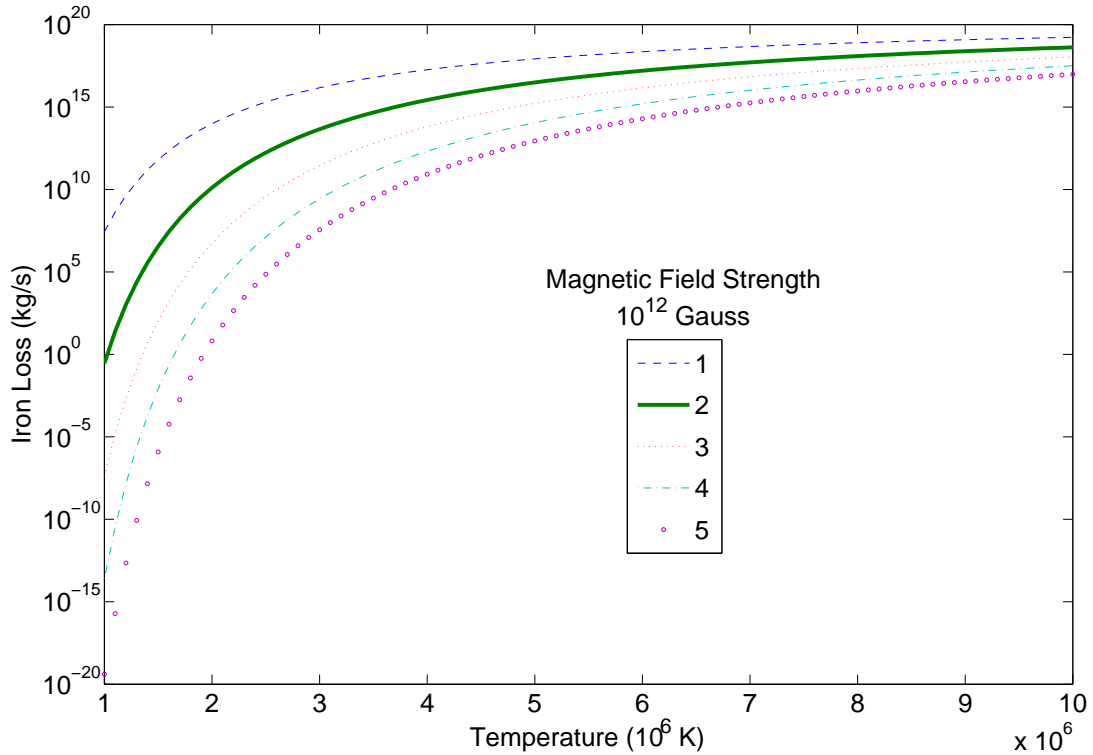
Figure 6: Loss rates for iron thermionically emitted from the polar cap region of the Crab pulsar, in kg/s. The bold line represents the Crab's magnetic field, 2×10^8 tesla. The sharp decline in significant emissions at temperatures lower than 10^6 K gives particular credence to Ruderman & Sutherland's argument that the general population of neutron stars is unable to release heavy nuclei positive ions. Note that the mass loss is logarithmically-scaled.

conduction by the core.

Under this scenario, we assume that, for the first 10^3 years, the surface temperature may be approximated linearly with respect to time since the supernova event. This is supported by Tsuruta et al. (1972), Figure 7a, though their canonical neutron star has a mass of 1.3 $M_{\odot}$. Van Riper (1991) compares several models based on various equations of state, Figure 7b, utilizing a 1.4 $M_{\odot}$ neutron star, similar in mass to that in the Crab. We note that several of the models exhibit precipitous declines in temperature after only the first year of existence, which is worrisome for our assumption of linearity.

We may, however, estimate the present day surface temperature of the Crab Pulsar by using current measurements of its luminosity. Kaspi et al. (2006) report the bolometric luminosity as 2.7×10^{27} J/s. This means that the flux over the entire surface area of the neutron star (SA = $4\pi R^2 = 4\pi (15.6 \times 10^3)^2 = 3 \times 10^9$ m^2) is 8.83×10^{17} J/s/m^2, equivalent to an effective surface temperature of roughly 2×10^6 K if we use the blackbody approximation. On the Van Riper
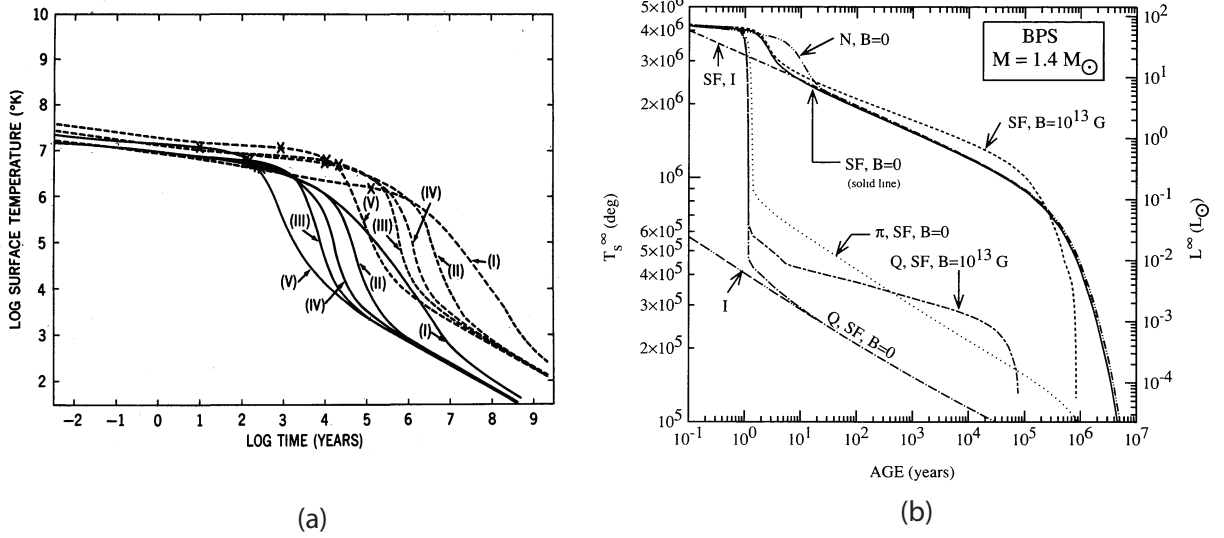
Figure 7: Various cooling models for the surface temperature of neutron stars. Figure (a) represents a 1.3 $M_\odot$ star, calculated for a wide number of possible interior equations of state. We are most interested in the fact that all models are generally linear up to 10^3 years. Reprinted from Tsuruta et al. (1972). Figure (b) utilizes a 1.4 $M_\odot$ star, like the Crab Pulsar, and presents a number of rapid cooling scenarios. Based on present observed temperature, however, the Crab pulsar is most like model (SF, I). Reprinted from Van Riper (1991).

diagram, Figure 7b, this places us on any one of several mostly linear models. As (N, B=0) and (SF, B=0) assume the absence of a magnetic field, we will not be using them; and, as our magnetic field is not quite 10^{13} gauss, we will use (SF, I), which is linear all the way until 10^5 years.

Thus, we estimate the temperature function as:

$$T(t) = 4 \times 10^6 - \frac{2 \times 10^6}{10^3}t \qquad (43)$$

$$= 4 \times 10^6 - 2 \times 10^3 t \text{ K}, \qquad (44)$$

where t is the age of the neutron star in years. We will now investigate two possible mechanisms by which the polar cap region may be heated in excess of the average surface temperature: irradiation by polar gap electrons, and Ohmic heating by subsurface currents.

5.2 Surface Irradiation by Polar Gap Electrons

As has been previously discussed, a vacuum gap exists above the polar cap region due to positron starving of the polar magnetosphere. Polar gap discharge occurs at a quasi-steady rate through the production of an avalanche of electron-positron pairs; the positrons refill the magnetosphere while the electrons are accelerated towards the surface. In the absence of significant surface conduction (Tsuruta et al. 1972, Jones 1978), these electrons should deliver a vast amount of energy to the surface ion lattice, raising its effective temperature.

19

As discussed above, electrons are drawn away from the surface of the neutron star via the electric fields generated by the rotating super-strong magnetic fields present near the surface. The departure of the electrons results in a net positive charge on the surface. Though the magnetosphere is also positively charged, the electric field at its base, a distance h from the neutron star surface, is zero. Electrons in the gap will be accelerated towards the surface, and it is reasonable to think of the magnetic polar cap region as a parallel plate capacitor. Inside the vacuum gap h a potential difference ΔV grows to a maximum:

$$\Delta V = \Omega B h^2, \tag{45}$$

where Ω is the angular frequency of rotation for the neutron star. We can use this potential to calculate the charge Q present on the surface:

$$Q = \frac{\epsilon_o (\Delta V) A}{h}. \tag{46}$$

Photons radiated from the surface are converted into numerous electron-positron pairs within the potential gap; this was the condition that allowed us to determine h via equation (30). The newly-formed electrons are attracted to the positively-charged surface and travel along magnetic field lines with a radius of curvature ρ. They release curvature radiation, which has energies $E_s \geq$ 1.022 MeV, sufficient to create additional electron-positron pairs. The curvature radiation/pair-production cycle continues until enough positrons have been produced that the magnetosphere is refilled and the potential gap collapses; that is to say, the amount of charge on the surface and the amount in the magnetosphere are the same.

Ruderman & Sutherland refer to this phenomenon as *sparking*. In the case of a very rapid rotator, like the Crab pulsar, sparking is extremely frequent and a nearly continuous flux of electrons irradiates the surface. In this limit, we may approximate the energy flux of the electrons, $\mathscr{F}_e$, as (Ruderman & Sutherland 1975):

$$\mathscr{F}_e = \tfrac{1}{2} \Delta V \rho_e \, c. \tag{47}$$

We will assume that the amount of conduction carrying heat away from the surface is negligible (Jones 1978). This is part of our assumption that the surface is in a state of thermal equilibrium, allowing us to use the blackbody approximation in order to determine the effective temperature of the surface. That is, all of the energy flowing into the surface through electron irradiation (or subsurface currents, discussed later) is matched by energy leaving the surface, in the form of electrons, positive ions or thermal radiation. ρ_e in equation (47) is the charge density that previously existed inside the vacuum gap and is now held on the surface as charge Q:

$$\rho_e = \frac{Q}{Ah}, \tag{48}$$

where A is the surface area of the magnetic polar region. The flux $\mathscr{F}_e$ is then:

$$\mathscr{F}_e = \tfrac{1}{2} \epsilon_o c \frac{(\Delta V)^2}{h^2} \tag{49}$$

$$= \tfrac{1}{2} \epsilon_o c (\Omega B h)^2. \tag{50}$$

The Crab pulsar has an angular frequency of:

$$\Omega = \frac{2\pi}{3.3 \times 10^{-2}} = 190 \, \tfrac{\text{rad}}{\text{sec}}, \tag{51}$$

20

so, from equation (50), $\mathscr{F}_e = 2.57 \times 10^{20}$ watts/m^2 for a gap width $h = 11.57$ m.

We are now concerned with the amount of energy lost by the electrons through synchrotron radiation processes. We are careful to distinguish synchrotron radiation, caused by the high velocity rotation of a charged particle in a magnetic field, with curvature radiation, the emission of photons caused by the acceleration of charged particles moving *along* curved field lines. The latter is singly identified as central to the formation of the polar electron avalanche by Ruderman & Sutherland. We now compare the synchrotron emissions of polar gap electrons to their kinetic energies.

We begin with the Larmor solution for a single electron moving in a magnetic field. In the electron's "rest" frame, the power radiated is:

$$P'_S = \frac{\mu_o e^2 a'^2_\perp}{6\pi c},\tag{52}$$

where $a'_\perp$ is the magnitude of the centripetal acceleration for the motion of the electron about a magnetic field line in the electron's frame. Given the ultrarelativistic motions of the electrons in this environment, along with the tightly confining superstrong magnetic field, we assume that the parallel component of the motion dominates the perpendicular (or circular) component: $v_\parallel >> v_\perp$. Under this assumption, $v_\parallel \approx v$, so conversion to the observer's frame involves:

$$a_\perp = \frac{a'_\perp}{\gamma^2}.\tag{53}$$

The power emitted by the electron in its frame is equivalent to the power eventually received by an observer (Rindler 1977):

$$P'_S = P_S .\tag{54}$$

Thus,

$$P_S = \frac{\mu_o e^2 a^2_\perp \gamma^4}{6\pi c},\tag{55}$$

which agrees with the solution given by Griffiths (1999).

Synchrotron motion is due to the centripetal acceleration of charged particles caused by the Lorentz force. The rotational motion may be described as follows:

$$a_\perp = \omega_S \cdot v_\perp,\tag{56}$$

where ω_S is the synchrotron frequency:

$$\omega_S = \frac{eB}{\gamma m_e},\tag{57}$$

so that:

$$a_\perp = \frac{eB}{\gamma m_e} v_\perp.\tag{58}$$

Here $v_\perp$ is the component of the electron's velocity perpendicular to the direction of the magnetic field. Acceleration in the polar gap, discussed elsewhere, brings electrons and positrons to near c

velocities *parallel to* the magnetic field. If we use the extreme assumption that the electrons travel at a total velocity $v = c$, then the condition $v^2 = v_\perp^2 + v_\parallel^2$ is satisfied by:

$$v_\parallel^2 = \left(1 - \frac{1}{\gamma^2}\right)c^2, \tag{59}$$

$$v_\perp^2 = \frac{c^2}{\gamma^2}. \tag{60}$$

This is equivalent to declaring that the pitch angle, θ, between the electron's velocity and the magnetic field is vanishingly small; electrons moving through the polar gap, like those found on the surface, are magnetically confined. This must be the case in this environment if any amount of electrons are going to reach the neutron star surface, a feature of the model discussed by numerous authors (Ruderman & Sutherland 1975, Jones 1978, Kaspi et al. 2006). Given this situation, the perpendicular acceleration, equation (58), is expressed as:

$$a_\perp = \frac{eBc}{\gamma^2 m_e}. \tag{61}$$

Using equation (61) in equation (55) yields:

$$P_S = \frac{\mu_o e^4 B^2 c}{6\pi m_e^2}. \tag{62}$$

The total synchrotron power for electrons formed above the polar cap of the Crab pulsar is 632 watts per electron in the limit $v = c$.

This represents the maximum amount of power that an electron undergoing synchrotron processes may generate in this environment; in reality, the electrons are traveling at total velocities less than c, so their perpendicular velocity will be less than $\frac{c}{\gamma}$. We are interested in how the energy radiated by the electrons through synchrotron processes as they traverse the polar gap, a maximum distance of $h = 11.57$ m, relates to their relativistic kinetic energy:

$$\begin{aligned} KE &= mc^2 - m_o c^2 \tag{63} \\ &= \gamma m_o c^2 - m_o c^2 \tag{64} \\ &= 1.80 \times 10^{-6} \text{ J} \tag{65} \end{aligned}$$

for Lorentz factor $\gamma = 2.2 \times 10^7$. The maximum synchrotron energy they could radiate in this magnetic regime is:

$$\begin{aligned} E_S &= P_S \cdot \frac{h}{v} \tag{66} \\ &= \frac{\mu_o e^4 B^2 h}{6\pi m_e^2}\left(1 - \frac{1}{\gamma^2}\right)^{-1/2}, \tag{67} \end{aligned}$$

which is practically constant for $\gamma \gg 1$.

Note that for electrons that are not so strongly confined:

$$a_\perp = \frac{eB}{\gamma m_e}v_\perp \tag{68}$$

22

$$= \frac{eB}{\gamma m_e} v \sin \theta, \tag{69}$$

$$P_s = \frac{\mu_o e^4 B^2 \gamma^2 v^2}{6\pi m_e^2 c} \sin^2 \theta, \tag{70}$$

$$E_s = \frac{\mu_o e^4 B^2 \gamma^2 h v}{6\pi m_e^2 c} \sin^2 \theta, \tag{71}$$

which would have much, much larger pitch angles, θ; this recovers the standard synchrotron theory result that $P_s \propto B^2 \gamma^2$ for highly relativistic electrons.

Figure 8 plots the kinetic energy of the electrons [equation (64)] and their maximum synchrotron radiated energy [equation (67)] as functions of γ for values $10 - (7 \times 10^9)$. These values of γ maintain the limit that total $v \approx c$. The figure demonstrates that, even with our tightly confined
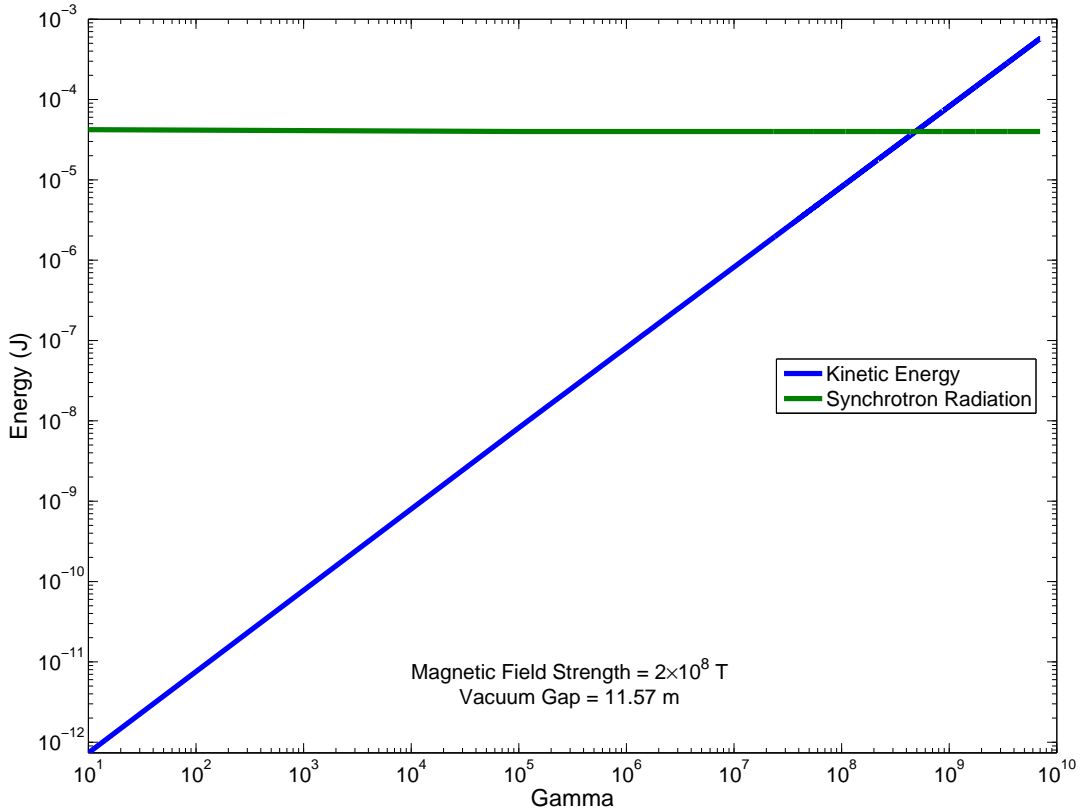

Figure 8: Comparison of kinetic and synchrotron energies for radiating electrons moving in the limit $v \approx c$. Electrons are produced in the polar gap at a maximum of 11.57 meters above the surface of the Crab pulsar and are rapidly accelerated to γ values in excess of 10^7. These lines represent the kinetic energy provided to and synchrotron losses for electrons maximally accelerated across the entire gap width; of course, this does not reflect the entire population of electrons created through pair production in the gap. Note that both axes are logarithmic.

motions, synchrotron radiation represents a significant drain on electron kinetic energies for a very wide range of Lorentz factor values. The break even point does not occur until around $\gamma = 5 \times 10^8$. We are currently unsure of the exact ramifications of this result: it seems unlikely that the electrons, having expended their entire kinetic energy reserves, will simply stop in the vacuum gap. They remain subject to the same accelerating forces that originally brought them to ultrarelativistic velocities. We have not currently considered treating the synchrotron process as a relativistic radiation reaction force, as may be necessary.

What is clear, however, is that nearly all of the energy lost by the electrons will be deposited on the polar cap surface because of relativistic beaming effects. The relativistic aberration of light by a point mass moving on a line is given by the expression (Walker 2007):

$$\cos \phi' = \frac{\cos \phi - \frac{v}{c}}{1 - \frac{v}{c} \cos \phi}, \tag{72}$$

where ϕ is the angle away from the particle's motion in which it emits radiation and ϕ' is the angle away from the particle's motion that the radiation is observed. In this way, 90% of the radiation emitted by an electron travelling at $\gamma = 2.2 \times 10^3$, 11.57 meters above the polar cap, is focused into a circle of area $2.19 \times 10^{-6} \text{m}^2$ on the surface. The electrons created in the Crab pulsar polar gap will focus their radiation into an even smaller area; thus, very little energy lost by these electrons through synchrotron processes will fail to reach the polar surface. In this way, we consider the electron flux determined via equation 50, $\mathscr{F}_e = 2.57 \times 10^{20}$ W/m^2, to be a valid indication of energy deposited on the surface. If we assume, as stated previously, that the surface is in quasi-thermal equilibrium, then all of this energy is eventually re-radiated and we will make use of the blackbody approximation, equation (78), to determine the effective temperature of the surface caused by electron irradiation. *Based on our calculated value for $\mathscr{F}_e$, the energy deposited by the falling electrons raises the surface temperature by a substantial 8.2×10^6 K.*

5.3 Ohmic Heating of the Surface

Recall from our pulsar model that the separation of charges in the magnetosphere induces the motion of charged particles in the subsurface layers of the neutron star. These are primarily electron flows, moving from the polar cap region towards the equator. Interestingly, the expression which Ruderman & Sutherland (1975) give for this "ion loss" is identical in magnitude to Michel's (1975) current leaving the surface via open field lines, $I = -2\kappa\epsilon_o R^3 B\omega^2$ (equation 5).

The surface of a neutron star is very similar to a sheet of metal, so we have reason to think that electrical currents flowing through it would produce heat via the Joule power law, expressed as an energy flux:

$$\mathscr{F}_c = \frac{P}{A} = \frac{I^2 \mathbb{R}}{A}, \tag{73}$$

where $\mathbb{R}$ is resistance. The current, equation (5), was derived by multiplying the charge density flowing from the polar cap by its area and c, so that:

$$I = \rho_s A c \tag{74}$$

Using this in equation (73), we see that the energy flux due to the current is:

$$\mathscr{F}_c = \rho_s^2 A \mathbb{R} c^2 \tag{75}$$

$$= 4\epsilon_o^2 \omega^2 B^2 A \mathbb{R} c^2 \qquad (76)$$

$$= 4\kappa\epsilon_o^2 c\omega^3 B^2 R^3 \mathbb{R} \qquad (77)$$

when we use equation (3) for the polar cap area. Using the standard Crab pulsar values, we have an expression for the heat generated in the polar cap as a function of the surface resistance: $\mathscr{F}_c = 1.68 \times 10^{23}\ \mathbb{R}$ J/s/m^2. We are not in possession of an exact value for $\mathbb{R}$, but we do know that resistance is inversely proportional to electrical conductivity, σ. As the subsurface currents serve to anchor the magnetic field to the surface, we know that σ must be very large (van den Heuvel 2006). Therefore, we will be using $\mathbb{R} = 1\ \mu\Omega$ in the crust. The flux associated with the currents (equation 77) is then roughly 1.68×10^{17} J/s/m^2, some three orders of magnitude less than the irradiation energy flux.

Combining the fluxes generated by surface electron irradiation, $\mathscr{F}_e$, and subsurface electron currents, $\mathscr{F}_c$, with the baseline flux determined by luminosity observations, $\mathscr{F}_o$, allows us to determine the effective temperature T_{eff} of the polar cap region, essential for the Jones thermionic emission function (equation 41). The combined flux is $\mathscr{F} = \mathscr{F}_o + \mathscr{F}_e + \mathscr{F}_c = (.883 + 257 + .168) \times 10^{18} = 2.58 \times 10^{20}$ J/s/m^2 emitted from the polar cap region of the pulsar. Using the blackbody approximation,

$$\mathscr{F} = \sigma T_{eff}^4, \qquad (78)$$

reveals that electron irradiation and subsurface currents (primarily the former) elevate the present surface temperature in the polar cap to $T_{eff} \approx 8.21 \times 10^6$ K, a 313% increase over the average temperature of the rest of the neutron star surface. Returning to Figure 6, which plots the rates of iron emission from the polar cap, in part as a function of temperature, suggests that the thousand-year-old Crab Pulsar is still capable of emitting iron at prodigious rates.

6 Concluding Discussion

Figure 6 is important for its suggestion that young, hot neutron stars behave as sources of significant amounts of positive ions before they cool to the critical temperature of $10^6 K$. At this temperature and below, though thermionic emission still takes place, it does so in drastically smaller quantities: if a Crab-like neutron star remained at 2×10^6 K for 1000 years it would release roughly 10^{10} kg of iron from its surface, while the same star emitting at 10^6 K for 1000 years would release only 1 kg. More importantly, we should into account the probability that the neutron star surface, as previously discussed, is not an isothermal environment. Figure 6 could then represent the rates for different locations on the surface, or even the same location at different times in the star's history. We are now concerned with the thermal history of the polar cap region.

In addition to the two heating processes that we have investigated, the surface is continually radiating energy away in the form of γ-rays. We assumed a linear relationship between surface temperature and stellar age that resulted in equation (44), which we must now modify in light of the irradiating polar gap electrons and subsurface currents acting as heat sources. If we assume that these processes do not vary significantly while the neutron star is young (that is to say, the Crab Pulsar is currently spinning at roughly the same rate as it was at its inception) then a constant 2.58×10^{20} J/s/m^2 is injected into the surface. This assumption, however, is clearly not the case, as rotational energy is tapped for overall nebular synchrotron radiation. A younger, more rapidly
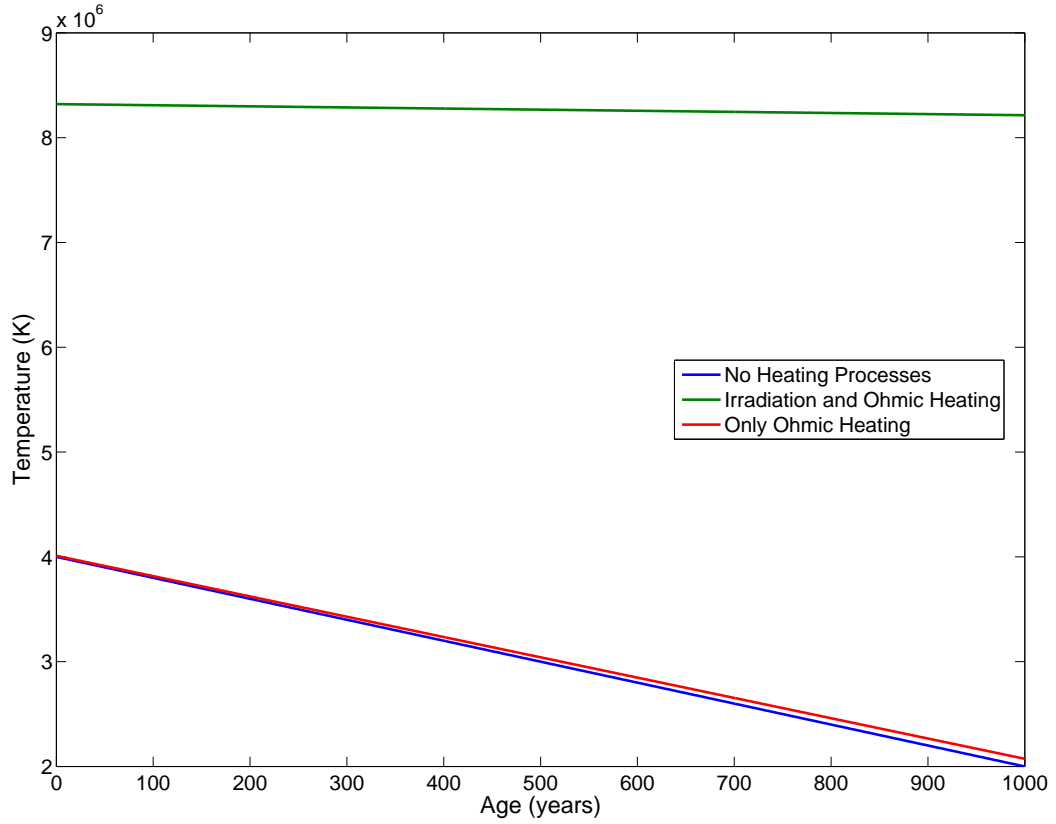
Figure 9: The linear cooling of the polar cap surface of a neutron star without active heating processes, with just subsurface Ohmic heating and with both Ohmic heating and irradiation by electrons formed in the polar gap. This figure clearly demonstrates that the heating caused by subsurface currents, which alone would only be significant in an older pulsar, is dominated by that from electron irradiation. Note the temperature is scaled to 10^6 K.

rotating Crab would be capable of even greater particle acceleration in the polar gap and stronger subsurface currents. We are thus calculating a lower limit on the iron mass lost.

Based on our computed polar surface temperatures, as well as the assumed constant energy inflow, the modified temperature relationship for the polar cap is then:

$$T(t) = 8.32 \times 10^6 - 106t \ \ \text{K}, \tag{79}$$

where t is once again the age of the pulsar in years. Figure 9 illustrates the effect of the additional heat: not only does the pulsar begin warmer, the overall rate of cooling is drastically diminished. In fact, the surface temperature in the polar cap is only reduced by roughly 1% in the presence of energy bombardment by electrons. If we use our modified temperature function in the Jones ionic emission rate formula, equation (41), we can express the ionic emission rate for the Crab Pulsar as

a function of time:

$$\Gamma = 1.46 \times 10^{39} \exp\left(\frac{-4.22 \times 10^3}{k_B T}\right) \tag{80}$$

$$= 1.46 \times 10^{39} \exp\left(\frac{-4.9 \times 10^7}{T}\right) \tag{81}$$

$$= 1.46 \times 10^{39} \exp\left(\frac{-4.9 \times 10^7}{8.32 \times 10^6 - 106t}\right) \text{ ions/s/m}^2, \tag{82}$$

where t is in years. Using the appropriate factors, this is easily converted to kg/s:

$$\Gamma A = 5.58 \times 10^{20} \exp\left(-\frac{4.9 \times 10^7}{8.32 \times 10^6 - 106t}\right) \text{ kg/s}, \tag{83}$$

expressing the amount of iron emitted from the polar cap region, as plotted in Figure 10. To determine the total amount of iron blown into space since the neutron star's formation, G, we need only convert ΓA into kg/year and compute the straightforward integral:

$$G = \int_0^{1000} \Gamma A dt \tag{84}$$

$$= \int_0^{1000} 1.77 \times 10^{28} \exp\left(\frac{-4.9 \times 10^7}{8.32 \times 10^6 - 106t}\right) dt \tag{85}$$

$$= 4.72 \times 10^{28} \text{ kg} = 2.38 \times 10^{-2} \, M_\odot. \tag{86}$$

In establishing a not-insignificant value for G, we are in a position to affirm one of our primary questions: whether or not heavy positive ions may be lifted from the surface of a neutron star. We have done so, however, in the framework of a pulsar model that has at its foundations the constraint that positive ions are not lifted from the stellar surface. Our investigation focuses on the possible exception offered by the model's architects, that neutron stars which are young enough may have sufficient thermal energy to "boil" ions from the surface. We have interpreted their notion of boiling as thermionic emission. This process is highly sensitive to temperature within the range in which neutron stars exist, leading us to uncover two processes by which the surface temperature may be sufficiently bolstered.

Of the two, ohmic heating by subsurface currents and irradiation by polar gap electrons, the latter dominates, as reflected in Figure 9. At present, the energy provided by infalling electrons raises the polar cap surface temperature by over 8×10^6 K, more than 6 times as much as Ohmic heating. Electron irradiation is also the one process of the two that is a consequence of the specific Ruderman & Sutherland model we adopted. Its authors strongly argue against the departure of positive ions from the neutron star surface, except possibly in the case of the Crab pulsar. We now consider the implications of deviating from the model.

In the worst case, the flow of positive ions from the surface into the polar magnetosphere would stunt the development of a full vacuum gap, which would in turn limit the amount of curvature radiation emitted by polar electrons. This would mean a net result of fewer electrons impacting the surface, allowing it to cool more rapidly and lowering the number of positive ions released into the gap. With the release of fewer positive ions, the gap could once again develop, increasing the electron energy flux onto the surface. Though it seems somewhat circular, Ruderman & Sutherland
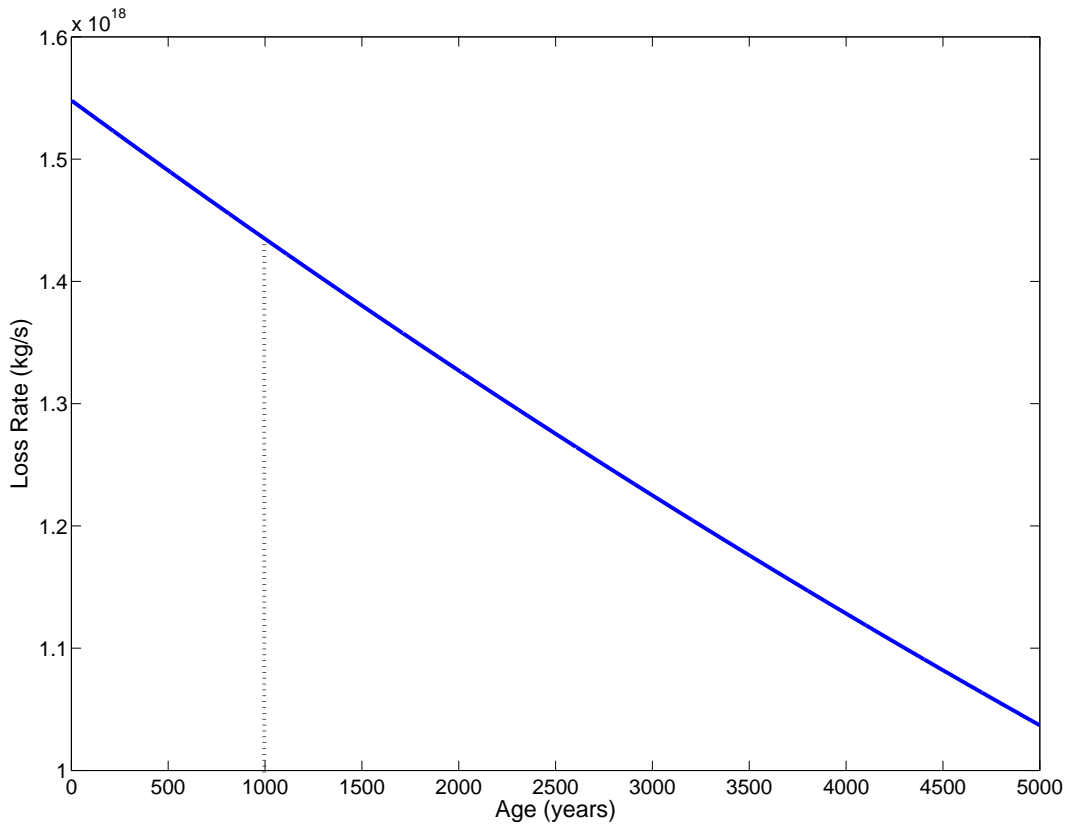
Figure 10: The decline in the rate of iron emissions as the surface of the Crab neutron star cools. After 1000 years, the current age of the Crab pulsar, the surface emits just above 1.4×10^{18} kilograms of iron per second. We note that the polar cap cools so slightly due to polar gap electron irradiation that this curve appears linear after 5000 years even though $(\Gamma A) \propto e^{-1/T}$. Note the scale of the loss rate is 10^{18} kg/s.

themselves say, "the $e^- - e^+$ discharge would be a necessary prerequisite for maintaining the surface temperature, therefore ... the gap must grow to a size sufficient for the electron-positron discharge to be maintained" (1975). Electron avalanches appear to be an inevitable aspect of this model, and it would seem that significant ionic emissions follow in their wake.

The thermal additions of Ohmic heating alone would be insufficient to maintain the temperature in the range of significant emissions throughout a neutron star's first 10^3 years, though the emission would continue to take place. It would appear that the environmental conditions of a young, Crab-like neutron star make the surface emission of iron nuclei highly likely. Our finding, 4.72×10^{28} kg, is likely an overestimate, but there are some compensating factors in the young pulsar that would keep it from being driven drastically lower: the stream of positive ions leaving the surface would limit the maximum size of the polar vacuum gap, but the increased rate of rotation would mean that the fewer number of electrons that are created would be accelerated to greater velocities. Regardless, even if positive ion streams completely choked-out the electron irradiation process, the

28

very young Crab pulsar, as indicated by Figure 6, would have been hot enough to thermionically emit a significant amount of iron for a number of years.

We note that there was recently a report of a localized very hot spot on the surface of the Crab pulsar (Weisskopf et al. 2004). Chandra X-ray observations initially suggested that the surface of the neutron star was 2.2×10^9 K. Even the young Crab would be unable to sustain this temperature across its entire surface, and Weisskopf and his collaborators interpreted the extreme temperature to represent a very small hot spot, possibly due to a second particle backheating mechanism. The temporary existence of these extremely hot spots would also bolster the primary emissions from the polar cap region, though more will have to be known about them (their surface area and lifespan) before we could estimate their contributions.

Finally, we reiterate that the calculations discussed here apply to iron ions, whereas we set out to investigate a possible mechanism for *nickel* enhancement in the nebular gas. This inconsistency is due to a lack of binding energy calculations in the literature for nickel and nuclei other than iron in the presence of super-strong magnetic fields. That said, nickel, as it would be found on the neutron star surface, only differs from iron by the addition of two protons and electrons. Their contributions to the binding ought to provide only slight increases in the cohesive energy. This means that the numbers for iron here presented should be approximations, specifically slight overestimates, of the amount of nickel leaving the neutron star surface. Its emission may also be complicated by the need to move upwards from the lower layers of the crust, where nickel is most likely to be found (De Blasio & Lazzari 1996). More specific nickel calculations, along with the ultimate directional distribution of positive ions freed from the surface, must remain for future investigations.

References

Cohen-Tannoudji, C., Diu, B., Laloë, F. 1977, *Quantum Mechanics*, trans. S. R. Hemley, N. Ostrowsky and D. Ostrowsky (Paris: Hermann and New York: John Wiley & Sons)

De Blasio, F. V., & Lazzari, G. 1996, ApJ, **468**, 346

Erber, T. 1966, Rev. Mod. Phys., **38**, 626

Fesen, R. A., & Kirschner, R. P. 1982, ApJ, **258**, 1

Flowers, E. G., Lee, J., Ruderman, M. A., Sutherland, P. G., Hillebrandt, W., Müller, E. 1977, ApJ, **215**, 291

Ginzburg, V. L. 1971, Soviet Physics Uspekhi, **14**, 83

Goldreich, P., & Julian, W. H. 1969, ApJ, **157**, 869

Griffiths, D. J. 1999, *Introduction to Electrodynamics*, 3rd ed. (Upper Saddle River: Prentice Hall)

Henry, R. B. C., MacAlpine, G. M., Kirshner, R. P. 1984, ApJ, **278**, 619

Jones, P. B. 1977, Nature, **270**, 37

Jones, P. B. 1978, Mon. Not. R. Astr. Soc., **192**, 847

Kaspi, V. M., Roberts, M. S. E., Harding, A. K. 2006, in *Compact Stellar X-Ray Sources*, ed. W. Lewin and M. van der Klis (Cambridge: Cambridge University Press), 279

Lyne, A. & Graham-Smith, F. 2006, in *Pulsar Astronomy* (Cambridge: Cambridge University Press)

MacAlpine, G. M., McGaugh, S. S., Mazzarella, J. M., Uomoto, A. 1989, ApJ, **342**, 364

MacAlpine, G. M., & Uomoto, A. 1991, AJ, **102**, 218

MacAlpine, G. M., Lawrence, S. L., Sears, R. L., Sosin, M. S., Henry, R. B. C. 1996, ApJ, **463**, 650

MacAlpine, G. M., Ecklund, T. C., Lester, W. R., Vanderveer, S. J., Strolger, L. 2007, AJ, **133**, 81

Michel, F. C. 1975, ApJ, **198**, 683

Miller, J. S. 1978, ApJ, **220**, 490

Nomoto, K. 1985, in *The Crab Nebula and Related Supernova Remnants*, ed. Kafatos and Henry (Cambridge: Cambridge University Press)

Protheroe, R. J., Bednarek, W., Luo, Q. 1998, Astroparticle Phys., **9**, 1

Rindler, W. 1977, *Essential Relativity*, 2nd ed. (New York: Springer-Verlag)

Ruderman, M. A. 1971, Phys. Rev. Letters, **27**, 1306

Ruderman, M. A., & Sutherland, P. G. 1975, ApJ, **196**, 51

Tsuruta, S., Canuto, V., Lodenquai, J., Ruderman, M. A. 1972, ApJ, **176**, 739

Uomoto, A., & MacAlpine, G. M. 1987, AJ, **93** 1511

van den Huevel, P. J. 2006, Science, **312** 539

Van Riper, K. A. 1991, ApJ Supplement Series, **75**, 449

Walker, J. 2007, "C-Ship: The Abberation of Light" in *Fourmilab*. Retrieved April 18, 2007, from http://www.fourmilab.ch/cship/aberration.html

Weisskopf, M. C., O'Dell, S. L., Paerels, F., Elsner, R. F., Becker, W., Tennant, A. F., Swartz, D. A. 2004, ApJ, **601** 1050